JVI Journals.ASM.org

Dynamic Interactions between *Bombyx mori* Nucleopolyhedrovirus and Its Host Cells Revealed by Transcriptome Analysis

Jian Xue,[a] Nan Qiao,[b,c,d] Wei Zhang,[b,c,d] Ruo-Lin Cheng,[a] Xiao-Qin Zhang,[a] Yan-Yuan Bao,[a] Yi-Peng Xu,[a] Lin-Zhu Gu,[a] Jing-Dong Jackie Han,[b] and Chuan-Xi Zhang[a]

Institute of Insect Science, Zhejiang University, Hangzhou, China[a]; Chinese Academy of Sciences Key Laboratory of Computational Biology, Chinese Academy of Sciences-Max Planck Partner, Institute for Computational Biology, Shanghai Institutes for Biological Sciences, Chinese Academy of Sciences, Shanghai, China[b]; Center for Molecular Systems Biology, Institute of Genetics and Developmental Biology, Chinese Academy of Sciences, Beijing, China[c]; and The Graduate University of Chinese Academy of Sciences, Beijing, China[d]

Although microarray and expressed sequence tag (EST)-based approaches have been used to profile gene expression during baculovirus infection, the response of host genes to baculovirus infection and the interaction between baculovirus and its host remain largely unknown. To determine the host response to *Bombyx mori* nucleopolyhedrovirus infection and the dynamic interaction between the virus and its host, eight digital gene expression libraries were examined in a Bm5 cell line before infection and at 1.5, 3, 6, 12, 24, 48, and 96 h postinfection. Gene set enrichment analysis of differentially expressed genes at each time point following infection showed that gene sets including cytoskeleton, transcription, translation, energy metabolism, iron ion metabolism, and the ubiquitin-proteasome pathway were altered after viral infection. In addition, a time course depicting protein-protein interaction networks between the baculovirus and the host were constructed and revealed that viral proteins interact with a multitude of cellular machineries, such as the proteasome, cytoskeleton, and spliceosome. Several viral proteins, including IE2, CG30, PE38, and PK-1/2, were predicted to play key roles in mediating virus-host interactions. Based on these results, we tested the role of the ubiquitin-proteasome pathway and iron ion metabolism in the viral infection cycle. Treatment with a proteasome inhibitor and deferoxamine mesylate *in vitro* and *in vivo* confirmed that these pathways regulate viral infection. Taken together, these findings provide new insights into the interaction between the baculovirus and its host and identify molecular mechanisms that can be used to block viral infection and improve baculovirus expression systems.

Bombyx mori nucleopolyhedrovirus (BmNPV) is a member of *Baculoviridae*, which is a large family of enveloped viruses that contain a large, circular, double-stranded, supercoiled DNA genome (80 to 180 kb) that carries between 90 and 180 genes (56). The BmNPV genome is packaged into rod-shaped virions, which are produced in the host cell during late infection. Baculoviruses are pathogenic for invertebrates, particularly members of Insecta, such as orders of Lepidoptera, Hymenoptera, and Diptera. Baculoviruses can be utilized as versatile vectors for protein expression in both insect and mammalian cell lines (29). BmNPV has a 128-kb genome and carries more than 100 genes (19). The genomic content of BmNPV is similar to that of *Autographa californica* multicapsid NPV (AcMNPV) (20).

Upon entry into a cell, baculovirus must outcompete components of the cellular machinery for gene transcription and genome replication. In insect cells, baculovirus genes have four temporally regulated transcription phases in the infection process: immediate early, early, late, and very late. In the initial steps of viral infection, transcriptional activators elevate the expression of baculovirus genes, which is a process that requires no viral factors, allows the virus to establish infection, and selectively modulates certain categories of host genes. Additionally, the upregulation of cellular actin-related proteins facilitates the movement of the nucleocapsid through the cytoplasm, which is essential for controlling host gene expression and producing viral progeny (18, 44). The late transcription phase is focused mainly on DNA replication and structural gene expression. After the initiation of viral-DNA replication, there is a switch from early dependence on a host RNA polymerase II to a novel, virus-encoded RNA polymerase. Recently, important aspects of virion binding and fusion on the cellular surface, intracellular transportation, genetic material transportation, DNA replication and transcription, RNA translation, virion assembly, and secondary infection have been revealed. Conversely, host resistance strategies such as the immune system, apoptosis, and RNA interference, among others, serve to block viral infection (58).

Changes in host gene expression in response to baculovirus infection are of great interest. The sequencing of the first genome of a lepidopteran insect, the silkworm, greatly facilitated the study of global host genes in response to baculovirus infection. Iwanaga et al. (21) reported the upregulation of seven genes and downregulation of four genes in the early phase of infection by subtractive hybridization and Northern blot analysis. Using suppression subtractive hybridization (SSH), Bao et al. (4, 5) reported that a total of 100 genes might be involved in the host antiviral mechanism. Specifically, a total of 15 viral proteins show similarity to silkworm proteins, which are categorized into the following

Received 4 January 2012 **Accepted** 13 April 2012
Published ahead of print 24 April 2012
Address correspondence to Chuan-Xi Zhang, chxzhang@zju.edu.cn, or Jing-Dong Jackie Han, jdhan@picb.ac.cn.
J.X. and N.Q. contributed equally to this work.
Supplemental material for this article may be found at http://jvi.asm.org/.

doi:10.1128/JVI.07217-12

groups: DNA polymerases, protein kinases, inhibitors of apoptosis, ubiquitin, chitinase, ecdysteroid UDP-glucosyltransferase, superoxide dismutase, fibroblast growth factor, SNF2 homolog, desmoplakin, methyltransferase, cathepsin, and protein tyrosine phosphatase (26). A recent study analyzing the global transcriptional profile of host genes in the silkworm cell line 12 h after infection with BmNPV by oligonucleotide microarray reported that a total of 35 host genes were significantly upregulated and 17 downregulated (59). Salem et al. (60) found that gene sets related to protein trafficking and processing in the endoplasmic reticulum (ER) and the Golgi apparatus were affected by AcMNPV infection. Nonetheless, changes in the global gene expression pattern following the infection process and the resulting information are limited, and the interactions between baculovirus and the host remain largely unknown.

During viral infection, each process involves a series of protein-protein interactions (PPIs). Therefore, identifying these interactions may clarify the mechanisms controlling the viral infection program. To date, most of the PPI studies have been performed on AcMNPV and *Helicoverpa armigera* nucleopolyhedrovirus (HearNPV) (45). A total of 45 viral and 5 host genes have been reported as PPIs at present (45). However, no large-scale experimental data describing baculovirus and host interactions are available. To our knowledge, previous studies could not reveal the systematic program of viral infection due to limited technology and analysis methods.

In recent years, next-generation, high-throughput DNA sequencing techniques have provided fascinating opportunities in the life sciences and dramatically improved the efficiency and speed of gene discovery (3). For example, Illumina sequencing technology offers millions of sequence reads from a single instrument run. This capacity allows for gene expression profiling experiments with an improved dynamic range and considerable cost savings. In this study, to analyze genome-wide differential gene expression following BmNPV infection in Bm5 cells, we first assembled the transcriptome sequences using next-generation sequencing. Next, we adopted global approaches to analyze the changes in gene expression. Based on the results of our transcriptome analysis and predicted domain-domain interactions, we constructed a PPI network between baculovirus and host proteins. Finally, the roles of the ubiquitin-proteasome pathway and iron ion metabolism in the viral infection cycle were validated *in vitro* and *in vivo*.

MATERIALS AND METHODS

Silkworm, cell lines, and virus maintenance. Bm5 cells were maintained at 27°C in TC-100 insect medium (Gibco, NY) supplemented with 10% (vol/vol) fetal bovine serum (Gibco-BRL) (28). BmNPV (T3 strain) was proliferated in Bm5 cells. The silkworm *B. mori* Qiufeng × Baiyu was reared at 27°C on fresh mulberry leaves.

Virus interval infection and cell collection. Bm5 cells were collected as uninfected cells (UIC) and at different intervals after infection (1.5, 3, 6, 12, 24, 48, and 96 h postinfection [hpi]). Each sample was subsequently washed with diethylpyrocarbonate (DEPC)-treated phosphate-buffered saline (PBS) solution (137 mM NaCl, 2.68 mM KCl, 8.1 mM Na_2HPO_4, 1.47 mM KH_2PO_4 [pH 7.4]) three times, and total RNA was immediately extracted.

Chemicals. PS-341 (Bortezomib) was obtained from LC Laboratories (Woburn, MA) and dissolved in dimethyl sulfoxide (DMSO) at a concentration of 10 mM, and *N*-succinyl-Leu-Leu-Val-Tyr-amido-4-methylcoumarin (Ys substrate) and deferoxamine (DFO) mesylate were purchased from Sigma-Aldrich (St. Louis, MO).

cDNA library preparation and Illumina sequencing for transcriptome analysis. Total RNA was extracted using the SV Total RNA isolation system (Promega, WI) according to the manufacturer's protocol. To obtain complete gene expression information, RNA samples from all different time points (UIC, 1.5, 3, 6, 12, 24, 48, and 96 hpi) were pooled and used for transcriptome analysis. According to the Illumina manufacturer's instructions, poly(A)$^+$ RNA was purified from 20 μg of pooled total RNA using oligo(dT) magnetic beads and fragmented into short sequences in the presence of divalent cations at 94°C for 5 min. Next, the cleaved poly(A)$^+$ RNA was transcribed, and second-strand cDNA synthesis was performed. After end repair and ligation of adaptors, the products were amplified by PCR and purified using a QIAquick PCR purification kit to create a cDNA library.

The cDNA library was sequenced on the Illumina sequencing platform (GAII). The raw reads from the images were generated using Solexa GA pipeline 1.6. After the removal of low-quality reads, processed reads with an identity value of 95% and a coverage length of 100 bp were assembled using SOAP *de novo* software and clustered using TGI Clustering (TGICL) tools (3, 47). In order to obtain an accurate and complete sequence library, Bm5 cell line sequences were combined with three sequence libraries (*Bombyx mori* UniGene library from NCBI, *Bombyx mori* coding sequences [CDS] from Beijing Genomics Institute [BGI], and transcriptome sequences performed in-house [data not shown]) using the TGICL tool to serve as a reference (47). The combined sequences were subsequently analyzed by searching the GenBank database with the BLASTX algorithm (http://www.ncbi.nlm.nih.gov/). Gene Ontology (GO) and Kyoto Encyclopedia of Genes and Genomes (KEGG) annotations of the reference sequences were determined using Blast2go (http://www.blast2go.org/), and the reference whole-genome sequence (128,413 bp) of BmNPV T3 was downloaded from NCBI.

Digital gene expression (DGE) library preparation and sequencing. Total RNA was extracted from cell line samples using the SV Total RNA isolation system (Promega, WI). DGE libraries were prepared using the Illumina gene expression sample preparation kit. Briefly, poly(A)$^+$ RNA was purified from 6 μg of total RNA using oligo(dT) magnetic beads. Double-stranded cDNAs were directly synthesized on the poly(A)$^+$ RNA-bound beads and were digested with NlaIII. The fragmentized cDNAs containing 3′ ends were purified from the magnetic beads, and the Illumina adaptor 1 was added to the 5′ ends of these cDNA fragments. After digestion with MmeI, an enzyme that recognizes the junction of the Illumina adaptor 1 (sense: 5′ACACTCTTTCCCTACACGACGCTCTTCCG ATC3′) and the CATG site, 21-bp tags containing the adaptor 1 sequence were produced. Subsequently, the Illumina adaptor 2 (sense: 5′GATCGG AAGAGCGGTTCAGCAGGAATGCCGAG3′) was ligated to the 3′ end of the tags to create a tag library. The library was amplified by PCR for 15 cycles, and 85-bp strips were purified from 6% PAGE gels. Next, the single-stranded molecules were attached to the Illumina sequencing chip for sequencing, and adaptor 1 was used as the sequencing primer. Each tunnel of chip (flow cell) generated millions of raw tags with a length of 35 bp.

Analysis and mapping of DGE tags. To map the DGE tags, the raw sequencing data were filtered to remove low-quality tags (tags with unknown nucleotide, "N"), empty tags (no tag sequence between the adaptors), and tags with only one copy number (which might result from sequencing errors). For tag annotation, the clean tags containing CATG and 21-bp tag sequences were mapped to our transcriptome reference database, allowing no more than one nucleotide mismatch. The clean tags were designated unambiguous clean tags. For gene expression analysis, the number of unambiguous clean tags for each gene was calculated and normalized to TPM (number of transcripts per million clean tags).

PCA. To reveal the relationships between all samples according to gene expression patterns, we performed principal-component analysis (PCA) using the statistical software R (http://www.r-project.org). PCA is a mathematical procedure for reducing the dimensionality of data while

retaining as much of the variation present in the original data set as possible, which is suitable for gene expression profiling data analysis. The first component concentrates the greatest of the variance and thus extracts the maximum amount of information.

Evaluation of DGE libraries. The statistical package edgeR (http://www.bioconductor.org/packages/2.3/bioc/html/edgeR.html) was used to identify the differentially expressed genes (DEGs) between each time point postinfection and control (false-discovery rate [FDR] < 0.05) (55).

PPIs predicted between virus and host. To analyze PPIs between the virus and the host, we annotated specific domains of each virus and host protein by using Inter-ProScan. Then, we mapped them to the domain-domain interactions predicted with high confidence (42% of which is known to be true) or those observed in Protein Data Bank (PDB) crystal structures from the DOMINE database (http://domine.utdallas.edu/cgi-bin/Domine). Next, we constructed networks at each time point using the DEGs determined by edgeR. Other than the predicted domain-domain interactions, the network also includes PPIs from KEGG (24) and FlyBase (62) annotated interactions, and high-confidence STRING (22) (confidence score > 0.7) and IntNetDB (65) (likelihood ratio > 7) interactions. The Markov Clustering (MCL) algorithm (http://www.micans.org/mcl/) was subsequently used to find the modules (clusters) in the PPI network with the information obtained from DEGs, and enriched GO/KEGG functions were calculated within each cluster as described by Xia et al. (66).

qRT-PCR. To detect and quantify viral-DNA and host cDNA sequences, quantitative real-time PCR (qRT-PCR) was used. The primer sets for BmNPV-DNA and Bm5 cell line-cDNA amplifications are listed in Table S1 in the supplemental material. Total RNA was extracted from Bm5 cells, as described previously. *Bombyx 18S rRNA* and *GAPDH* genes were used as internal controls in cDNA and genomic DNA samples, respectively. Amplification and real-time detection of PCR products were performed with the ABI Prism 7500 Real-Time PCR system (Applied Biosystems, Foster City, CA) using the SYBR Premix *Ex Taq* kit (TaKaRa, Dalian, China) according to the manufacturer's protocol. Each amplification reaction was performed using a 20-μl reaction mixture under the following conditions: denaturation at 95°C for 30 s followed by 40 cycles of 95°C for 5 s and 60°C for 34 s. Following cycling, melting curves were constructed. The results were normalized to the expression level of the constitutive internal gene. A no-template control (NTC) sample (nuclease-free water) was included in the experiment to detect contamination and to determine the degree of dimer formation. A relative quantitative method (threshold cycle [$\Delta\Delta C_T$]) was used to evaluate the quantitative variation.

To confirm DEGs, total RNA samples were extracted as described for the DGE library preparation. The concentration of each RNA sample was adjusted to 1 μg/μl with nuclease-free water, and 2 μg of total RNA was reverse transcribed with random primer in a 20-μl reaction volume using the Quant reverse transcriptase kit (Tiangen, China). The *Bombyx 18S rRNA* gene was used as an internal control, and a total of 11 *Bombyx* genes were tested.

Proteasome inhibitor treatment. To determine if the ubiquitin-proteasome pathway is involved in the BmNPV infection, we treated Bm5 cells with a proteasome inhibitor, PS-341, at a concentration of 5 μM. Three milliliters of TC-100 medium, with or without PS-341, was added to 35-mm cell culture dishes, and each dish was infected with BmNPV at a multiplicity of infection (MOI) of 10 for 1 h at 27°C. Next, the infected cells were washed three times with TC-100 medium, and 3 ml of fresh TC-100 medium, with or without PS-341, was added. At different intervals, 100 μl of supernatant was removed, which was used to analyze budded virus (BV) genome copies. To assess the impact of PS-341 (5 μM) on BmNPV-DNA replication, Bm5 cells were treated at different intervals (0, 3, and 6 hpi). We also studied the transcription regulation of viral genes with proteasome inhibitor. PS-341 was added to the culture supernatant of virally infected cells at both 1.5 and 4.5 hpi. Total RNA samples were extracted at 6 and 12 hpi, and the cDNA was synthesized as described above. Two viral genes, the immediate-early gene *ie1* and the very late gene *polh*, were used to test the effects on gene expression. We also sought to identify the function of the ubiquitin-proteasome pathway *in vivo* in *B. mori* Qiufeng × Baiyu. BmNPV-infected fifth-instar larvae, with or without PS-341, were dissected, and hemocytes and fat bodies were collected at different time points (3, 6, 12, 24, 36, and 48 hpi). All experiments were performed in triplicate. Genomic DNA was extracted using the Universal Genomic DNA extraction kit Ver 3.0 (TaKaRa, Dalian, China). Next, the DNA samples obtained from hemocytes and fat bodies were evaluated by qRT-PCR. A pair of *DNApol* primers was designed according to the sequence of the BmNPV T3 *DNApol* gene, and *Bombyx GAPDH* was used as an internal control.

Proteasome activity assay. Bm5 cells were seeded in 35-mm cell culture dishes. After incubation for 1 day, the cells were treated with PS-341 (5 μM) and harvested at a series of time points (0.5, 1, 1.5, 3, and 6 h). Proteasome activity assays were also performed for hemocytes and fat bodies. Briefly, *B. mori* larvae were injected with PS-341 (10 μl of 0.5 mM PS-341 in DMSO), and tissue and cells were obtained at 6, 12, 24, and 48 h after treatment. Then, treated samples were subjected to fluorometric measurement of 20S proteasome activity assay using Ys substrate, as previously described with slight modifications (1, 68). After incubation at 37°C for 30 min, plates were read using a Synergy HT multidetection microplate reader (Bio-TEK) at an excitation wavelength of 380 nm and emission wavelength of 460 nm.

Treatment of iron ion binding reagent. To investigate the effect of iron ion on BmNPV T3 infection, we used DFO mesylate to bind free iron in cells. Bm5 cells were treated with DFO mesylate (0.05, 0.5, and 1 mM) for 1 day before BmNPV T3 infection, control cells were treated with distilled water (the diluents used for DFO mesylate), and virus DNA replication was assessed as described previously.

Cell mortality assay. After treatment with PS-341, DFO, or (for controls) DMSO or H_2O for 12, 24, 48, and 72 h, Bm5 cells were stained using a cell viability assay kit (Beyotime Institute of Biotechnology, China), and cell mortality was calculated in random visual fields.

Statistical analysis. Statistical comparisons among groups were performed with Student's *t* tests. *P* values of ≤ 0.05 were considered significant.

Nucleotide sequence accession numbers. The raw transcriptome and tag data have been deposited in SRA under accession numbers SRX098100 and SRX098087, respectively.

RESULTS

Reference sequence library construction and annotation. We were able to obtain 24,720 sequences with a mean reference data length of 1,042 bp. The N50, a statistical measure of average length of transcriptome library sequences, was 1,434 bp, and 88.6% of the sequences had a length of more than 300 bp. To annotate these sequences, BLASTX was used to search the nonredundant (nr) NCBI protein database for reference sequences with a cutoff E value of 10^{-5}. We found that a total of 17,433 sequences provided BLAST results (70.5% of all distinct sequences) (see Table S2 in the supplemental material). GO and KEGG annotations were subsequently used to classify the functions of these reference sequences. Our results revealed that a total of 4,106 GO and 251 KEGG gene sets had been annotated (see Table S2 in the supplemental material).

DGE library sequencing and quantitative gene expression data. Complete transcriptome profiles were compared at different time points (UIC, 1.5, 3, 6, 12, 24, 48, and 96 hpi) to generate between 3.1 and 4.1 million raw tags of these samples (see Table S3 in the supplemental material). After low-quality tags were removed, the total number of clean tags per sample ranged from 2.8 to 3.6 million (see Table S3 in the supplemental material). On

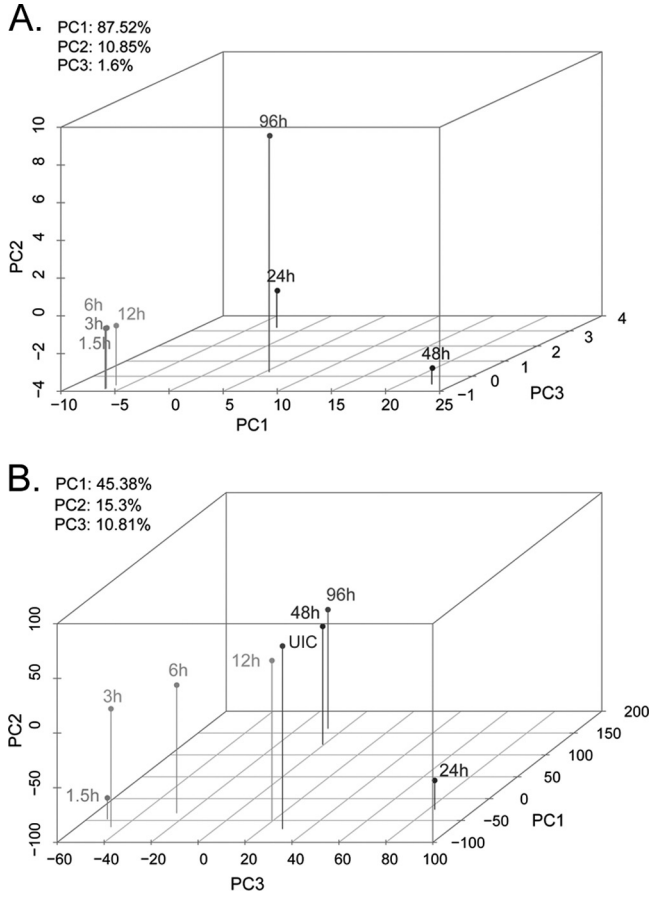

FIG 1 Principal component analysis (PCA) across libraries. The first three components from the principal component analysis, PC1, PC2, and PC3, define the *x*, *y*, and *z* axes of the 3-dimensional space, so the distance between any two points indicates the variances between them. Shown are 3-dimensional scatter plots of the PCA of viral genes (A) and of host genes (B).

average, 91.09% of the raw tags were found to be clean tags within a range of 86.87 to 94.93% (see Table S3 in the supplemental material). Furthermore, the percentage of unknown tags that could not be mapped to the reference library ranged from 3.76 to 8.61%, except for the samples collected at 48 and 96 hpi, which ranged from 67.05 to 78.18% (see Table S3 in the supplemental material). Saturation analysis demonstrated that the number of detected genes decreased as the number of sequence tags increased, and the capacity of the library reached saturation when the number of sequence tags approached 2.5 million (see Fig. S1 in the supplemental material). A total of 17,883 genes were mapped using clean tags (137 viral genes and 17,746 host genes).

Overall transcriptome variations among samples. To obtain an overview of the relationships among the eight samples, PCA was performed using the total gene expression profiles. PCA revealed the internal structure of the data in a way that best explained the variances in the data. The first three principal components, PCA1, PCA2, and PCA3, contribute a great percentage (99.97% for the viral data; 71.49% for the host data) of the total variability of the data when using a 3-dimensional scatter plot to plot the first three components of each time point (Fig. 1A and B). The time points varied according to the three largest variations in the data. Accordingly, we found that viral samples taken at 1.5, 3, 6, and 12 hpi only showed small variances, while the samples collected at 24, 48, and 96 hpi showed great variances (Fig. 1A). Comparatively, for the host samples, only small variances were observed between the samples taken at the last two time points (48 and 96 hpi).

Viral gene expression. All of the known BmNPV T3 genes were expressed upon infection of Bm5 cells (see Table S4 in the supplemental material). Consistent with previous reports, these genes could be classified into four transcription phases: immediate-early, early, late, and very late genes. According to the transcription start time calculated in our study, five different gene expression patterns were observed at each time point from 1.5 to 24 hpi, except for P47, in which expression was detected at only 48 hpi (Table 1 and Fig. 2). The following five genes, all of which are classified as immediate-early genes and are important for the function of transcription and translation, were expressed at 1.5 hpi: *ie0*, *ie1*, *ie2*, *me53*, and *pe38* (Table 1). A total of 14 genes began to express at 3 hpi (Table 1). According to previous studies, some of them are classified as early genes, such as *39k* and *arif1*, while others are classified as late genes, such as *lef11* and *odv-ec27*. Two genes, *lef11* and *dnahel*, are associated with viral-DNA replication, and several genes influence cell fate and host molting (*odv-ec27*, *fgf*, and *egt*). At 6 and 12 hpi, we observed the expression of 43 and 50 genes, respectively (Table 1), all of which belong

TABLE 1 Virus gene clusters according to transcription start time

Transcription start time (hpi)	No. of transcribed genes	Names of transcribed genes	Transcription phase(s)
1.5	5	*pe38*, *ie0*, *ie2*, *me53*, *ie1*	Immediate early
3	14	*orf4*, *39k*, *orf9*, *arif1*, *lef11*, *egt*, *orf14*, *odv-ec27*, *odv-e26*, *hel*, *dbp*, *fgf*, *gp64*, *orf20*	Early
6	43	*orf5*, *lef3*, *he65*, *chitinase*, *polyhedrin*, *ubiquitin*, *lef1*, *pk-2*, *orf99*, *orf101*, *lef7*, *lef6*, *p10*, *vp39*, *orf10*, *orf35*, *orf36*, *orf54*, *orf56*, *an*, *p35*, *lef9*, *bro-a*, *lef2*, *bro-c*, *bro-b*, *bro-e*, *bro-d*, *vp80*, *lef4*, *orf64*, *orf65*, *orf67*, *orf68*, *orf84*, *orf134*, *orf21*, *p26*, *orf41*, *orf46*, *dnapol*, *orf44*, *orf45*	Late and very late
12	50	*pkip*, *p94*, *pp34*, *vp91*, *iap1*, *odv-ec43*, *orf76*, *orf122*, *orf74*, *vp15*, *orf98*, *orf129*, *38k*, *iap2*, *orf17*, *orf109*, *orf59*, *p43*, *p12*, *orf34*, *orf51*, *p33*, *odv-e56*, *odv-e18*, *gta*, *gp41*, *lef10*, *pk-1*, *cathepsin*, *adprase*, *lef8*, *orf25*, *lef5*, *sod*, *orf60*, *orf61*, *orf62*, *odv-e66*, *vp1054*, *orf133*, *orf118*, *pif3*, *mtase*, *pif1*, *orf22a*, *orf94*, *orf96*, *odv-e25*, *odv-c42*, *cg30*	
24	24	*ets*, *gp37*, *gp16*, *orf90*, *orf93*, *dnaj*, *orf121*, *p74*, *orf58a*, *orf125*, *pif2*, *orf91*, *lef12*, *orf79*, *p78/83*, *ptp*, *orf42*, *vlf-1*, *p24*, *fp25k*, *pif4*, *chab1*, *p45*, *chab2*	
48	1	*p47*	

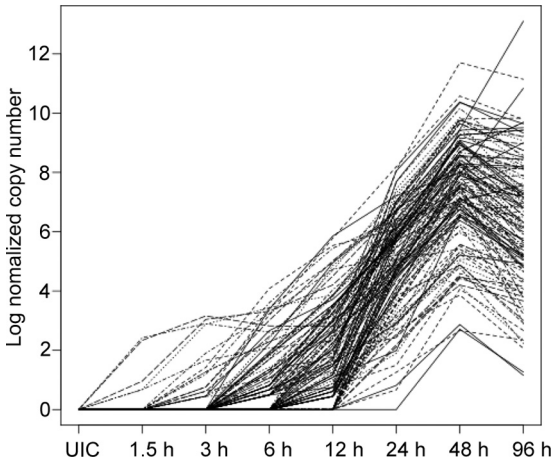

FIG 2 Viral gene expression patterns. Each viral gene expression pattern was graphed over time from the start of its expression. The *x* axis represents the time points after the virus infection, and the *y* axis represents the log-transformed viral gene copy number.

to the late and very late transcription phases and are associated with transcription, translation, structural protein, and inhibition of apoptosis in the host. The transcription of 24 genes started at 24 hpi (Table 1), and the expression of almost all viral genes peaked at 48 hpi and decreased within 96 hpi. As all of the viral genes were highly upregulated after infection, we further quantified the expression levels of host and viral genes. As shown in Fig. 3, the percentage of host cell mRNA transcription gradually decreased after 12 hpi and showed a marked decline at 48 hpi. The expression of viral genes was greatly increased at 48 and 96 hpi.

DEGs and cellular function changes across libraries. To ensure that the differences between gene expression profiles were related to the viral infection process, we compared all BmNPV infection samples with UIC (see Table S4 in the supplemental material and Fig. 4). As shown in Fig. 4, more than 1,000 genes were differentially expressed at 1.5 hpi compared to the control. A total of 637 of these genes were upregulated, and 448 genes were downregulated, suggesting that BmNPV infection has a strong effect on gene expression in this cell line. As for the expression patterns of samples collected at 3, 6, and 12 hpi, the numbers of differentially expressed UniGene clusters were much lower (3 hpi, 413; 6 hpi, 592; 12 hpi, 298) than observed for the 1.5 hpi sample. The majority of DEGs faded among these samples (Fig. 4); however, a subset of genes remained altered. A strong response was also observed at 24 hpi with a total of 1,169 UniGene clusters that were differentially expressed (Fig. 4), which might be attributed to the second wave of BmNPV infection. At 48 and 96 hpi, most of the host genes were downregulated (Fig. 4).

To gain further insight into the changes in cellular function across libraries, we performed functional analyses for these DEGs (Table 2; see also Table S5 in the supplemental material). The DEGs at 48 and 96 hpi were not considered because most of them were downregulated during these time points and, as a result, are not so useful in understanding the process of BmNPV infection. At 1.5 hpi, most upregulated genes were associated with transcription, translation, energy metabolism, cytoskeleton, ubiquitin-proteasome pathway, homeostasis, endopeptidase activity, and organism development. Alternatively, most of the downregulated gene sets were related to transcription, translation, cell cycle, mismatch repair, and protein metabolism. Some of these gene sets were both upregulated and downregulated, while a number of genes associated with the initiation of translation (eukaryotic translation initiation factor 3, 2B, and 1 complex) were dramatically upregulated. Similar expression patterns were observed at 3 hpi compared to the 1.5 hpi sample. Specially, we found that the following gene sets related to iron ion transport were upregulated at 3 hpi: iron ion transport, transition metal ion binding, ferric iron binding, and cellular iron ion homeostasis. Also, we observed similar results at 6 hpi, with upregulation of gene sets being associated with transcription, translation, ubiquitous-proteasome pathway, energy metabolism, iron ion transport, and organism development. At 12 hpi, the downregulation of translation initiation factor-associated gene sets was significantly enriched under the FDR threshold, and responses to stress gene sets were strongly upregulated. At 24 hpi treatment, gene sets primarily related to energy metabolism, homeostasis, and response to stress were found to be downregulated, and gene sets related to translational

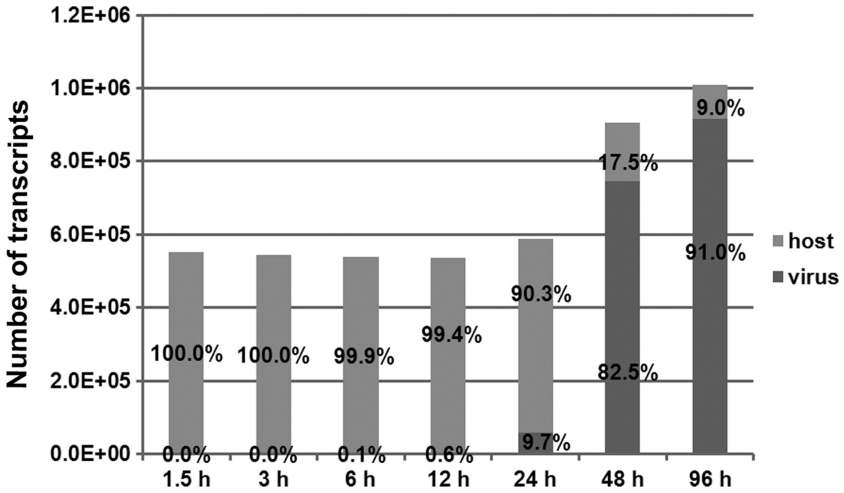

FIG 3 Percentages and total numbers of transcripts between virus and host cells over the course of infection. The numbers of viral and host cell transcripts were counted in different intervals on the *y* axis, and the percentages were calculated.

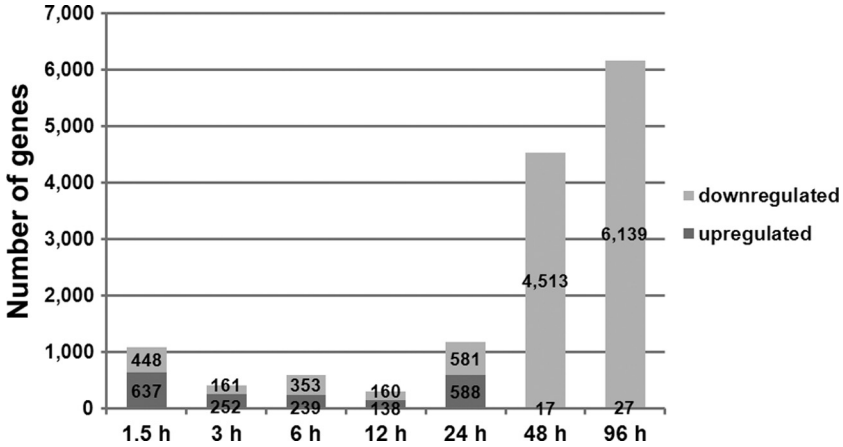

FIG 4 Number of host genes in each DGE comparison. The DEGs were identified using edgeR between each time point postinfection (1.5 hpi to 96 hpi) and control (FDR < 0.05). The numbers of upregulated and downregulated genes were determined.

initiation, mRNA splicing, protein metabolism, nucleosome, ubiquitin-proteasome pathway, energy metabolism, response to stress, and endopeptidase activity remained highly upregulated.

To confirm the validity of our gene profiles, the expression of various genes associated with the ubiquitin-proteasome pathway, spliceosome, transcription, translation, and nucleosome were examined by qRT-PCR. All of the genes examined exhibited overall expression patterns similar to those observed at different time points (see Fig. S2 in the supplemental material). Specifically the expressions of the following genes were validated: *proteasome subunit beta 5* (*PSMB5*) and *effete*, which are related to the ubiquitin-proteasome pathway; *small nuclear ribonucleoprotein polypeptide* (*SNRP*) and *LSM4 homolog* (*U6*), which are components of the spliceosome; *eukaryotic translation initiation factor 3 subunit 6* (*eIF3-6*), *eukaryotic translation initiation factor 1A* (*eIF1A*), *elongation factor 1 delta* (*EF1d*), and *eukaryotic translation initiation factor 3 subunit 2 beta* (*EIF3-2b*), which are associated with transcription and translation; and *histone H2A-like protein 2* (*H2A-l2*), *histone H2A variant* (*His2Av*), and *histone H3.3A* (*H3.3A*), which are related to histones. Overall, these results were consistent with those of our DGE analysis.

Prediction of BmNPV and host PPI network. Our PPI predictions identified 8,907 interactions between BmNPV and silkworm proteins. Among these genes, 22 viral genes were predicted to interact with 2,326 host genes. Also, 147 host genes were predicted to interact with greater than 10 viral genes (see Table S6 in the supplemental material), most of which were related to immune signaling pathways, cell cycle, and transcription.

Next, we constructed a subnetwork for each time point using the DEGs determined by edgeR (see Fig. S3 in the supplemental

TABLE 2 Numbers of differentially expressed genes in gene set categories[a]

	1.5 hpi		3 hpi		6 hpi		12 hpi		24 hpi	
Gene function	Up	Down	Up	Down	Up	Down	Up	Down	Up	Down
Transcription	6	51		26	2	48	2	21	10	
Translation	63	26	36	18	36	7	21	23	55	23
Translation initiation	12		6		4		3	4		
Translation elongation	3		2						3	
mRNA splicing	15	6	6		5	6			17	
Protein metabolism	17	6	6		8	11	5	7	17	3
Nucleosome	4				3		2		5	
Chromatin		4							3	
Mismatch repair		3								
Mitosis	9	5	11	5	8	5	4	4	9	8
Cell cycle		3		5				3		
Ubiquitin-proteasome	26		14		12		5		20	
Energy metabolism	42		23		32		21		32	17
Cytoskeleton	8		8		2					
Ion transport			3		3					
Homeostasis	6									7
Response to stress			4		2		10		11	7
Endopeptidase activity	10		7		6		3		10	
Glycosylation	2								2	
Organism development	5		17		11	3	3		7	
Others	105	60	67	25	97	73	46	39	78	45

[a] Values represent the number of genes regulated in gene set categories. Up, upregulated; down, downregulated.

material) and observed that IE2, CG30, PE38, and PK-1/2 carried the most virus-host PPIs. Other viral proteins (ubiquitin, PTP, chitinase, DNApol, FGF, GTA, IAP1/2, SOD, MTase, etc.) also interacted with host proteins. Then, we performed the MCL algorithm to identify network modules (densely connected regions) within PPI networks and calculated enriched functions, providing an indication of the functional diversity of each module (see Table S7 in the supplemental material). These results are reflective of the mechanisms involved in virus and host protein interactions. At 1.5 hpi, viral proteins of IE1, IE2, and PE38 were clustered in the same module, and this module was enriched in the ubiquitin-proteasome pathway. Next, at 6 hpi, the module contained IE2 and PE38, which regulate multiple functions involved in the ubiquitin-proteasome pathway, mitogen-activated protein kinase (MAPK) signaling pathway, cell cycle, and antiapoptosis. PE38, IE2, PK-1, and GTA were found to be in the same module at both 12 and 24 hpi. We observed that these gene sets were mainly involved in cell cycle, host responses to stress, nucleic acid metabolism, and ubiquitin-proteasome pathway (i.e., cell cycle, spliceosomal complex, Jun N-terminal protein kinase [JNK] cascade, RNA processing, and response to stress).

Among the tested infection intervals, 24 hpi is the most important time point for viral infection and showed the greatest number of interactions between viral and host proteins in one module (Fig. 5A). A total of eight subnetworks were separated from the module according to gene set functions with a *P* value of less than 0.05. The functional activities of these subnetworks are involved in transcription, protein metabolism, the spliceosome, the nucleosome, stress response, actin assembly, mitosis, and immunity (Fig. 5B through I). Additionally, 11 viral proteins, including MTase, GTA, PK-2, PK-1, PE38, IE2, IAP2, PTP, DNApol, ubiquitin, and GP41, were involved in interactions. Considering that the ubiquitin-proteasome pathway is significantly enriched at most of the infection intervals, we selected the differentially expressed ubiquitin-proteasome pathway genes from each infection interval. The interactions between viral and host proteins, including IE2, PE38, PK-1, PK-2, ubiquitin, and CG30, increased as infection proceeded (Fig. 6).

Identification of proteasomal function. The ubiquitin-proteasome pathway is involved in diverse cellular functions and has been shown to be important to the viral life cycle (23). Considering that ubiquitin-proteasome pathway-related gene sets are strongly upregulated after BmNPV infection, we suspected that BmNPV requires this cellular machinery to facilitate infection. No obvious cytotoxicity was observed in PS-341 and control treatments at the indicated time courses (Fig. 7A). Similarly, propidium iodide staining revealed no difference in the number of apoptotic cells following treatment with the inhibitor or DMSO (data not shown). To test our hypothesis, we used qRT-PCR to monitor the dynamic BV copies in Bm5 cell culture supernatants, viral-DNA proliferation in Bm5 cells, and hemocyte and fat body levels in response to proteasome inhibitor treatment. PS-341 effectively inhibited 20S proteasome activity immediately after treatment, both *in vitro* and *in vivo* (Fig. 7B and C). Over the course of infection, BV copies were dramatically increased in control cells after 24 hpi (Fig. 7D). In contrast, BV proliferation remained low in the inhibitor-treated samples (Fig. 7D). Furthermore, with the inhibitor treatment, viral-DNA replication in Bm5 cells had a great decrease at each time point after inhibitor treatment (Fig. 7E), similar to the pattern observed for BV copy changes. We further characterized the effect of proteasome inhibition on viral gene transcriptions. Transcriptions of both the immediate-early gene *ie1* and the very late gene *polh* were downregulated with PS-341 treatment at 1.5 and 4.5 hpi (Fig. 7F). Moreover, occlusion-derived virus (ODV) production in Bm5 cells was extremely restricted following PS-341 treatment (Fig. 8A, C, and E). To study this effect *in vivo*, *B. mori* larvae were treated with PS-341, and the results showed that viral-DNA proliferation was inhibited in hemocytes and fat bodies at 6, 12, 24, 36, and 48 hpi (Fig. 7G and H).

Identification of iron ion metabolism. In the early infection phase (3 and 6 hpi), we observed that gene sets related to iron ion metabolism (i.e., iron ion transport, ferric iron binding, and cellular iron ion homeostasis) were highly upregulated after BmNPV infection. To determine whether iron ion metabolism influences BmNPV infection, DFO mesylate was added to media to bind free iron in cells, and qRT-PCR was used to quantify the amount of viral-DNA in Bm5 cells after 12, 24, and 48 hpi. Similar to PS-341, DFO also showed no obvious cytotoxicity to Bm5 cells during the test (Fig. 9A). As shown in Fig. 9B, DFO mesylate efficiently blocked BmNPV-DNA replication after internalization at the intervals examined, which showed a dose-dependent inhibition of viral-DNA yield in Bm5 cells. In contrast, no effect was observed in control-treated cells (Fig. 9B). Meanwhile, DFO treatment of Bm5 cells kept them as stable as normal cells at 48 hpi (Fig. 8B, D, and F).

DISCUSSION

In previous studies, gene expression profiling analysis of host and NPV gene transcription has been performed at different infection intervals (36, 41, 59, 60). However, due to limited data, the enrichment of DEG sets could not be determined, and further analysis could not be performed. In this study, we obtained a global expression profile for the BmNPV infection process by using next-generation sequencing and transcriptome sequences as a reference library. To our knowledge, this study represents the most comprehensive and accurate gene expression profiling for a baculovirus infection process to date. Gene enrichment studies and further analysis showed that BmNPV infection causes rapid and violent transcriptional responses in cells at 1.5, 24, 48, and 96 hpi and reduced transcription at 3, 6, and 12 hpi. According to gene expression kinetics, the peak responses appeared at 1.5 and 24 hpi. However, at later time points following viral infection, the expression of most host genes was inhibited (Fig. 4). Many genes related to transcription, mismatch repair, translation, cell cycle arrest, energy metabolism, cytoskeleton, protein metabolism, and the ubiquitin-proteasome pathway were modulated during the infection process.

The ubiquitin-proteasome pathway is required for virus replication and transcription. The ubiquitin-proteasome pathway is a major regulator of intracellular protein levels and plays an important role in viral infections through the avoidance of host immune surveillance, viral progeny release and budding, transcriptional regulation of the virus, and suppression of apoptosis (17, 25). We observed that genes related to the ubiquitin-proteasome pathway were upregulated throughout the course of the infection (Table 2; see also Table S5 in the supplemental material). Network analysis also revealed that viral proteins interact with multiple host proteins in the ubiquitin-proteasome pathway (Fig. 6). Specifically, PE38, IE2, PK1, PK2, ubiquitin, and CG30 were pre-

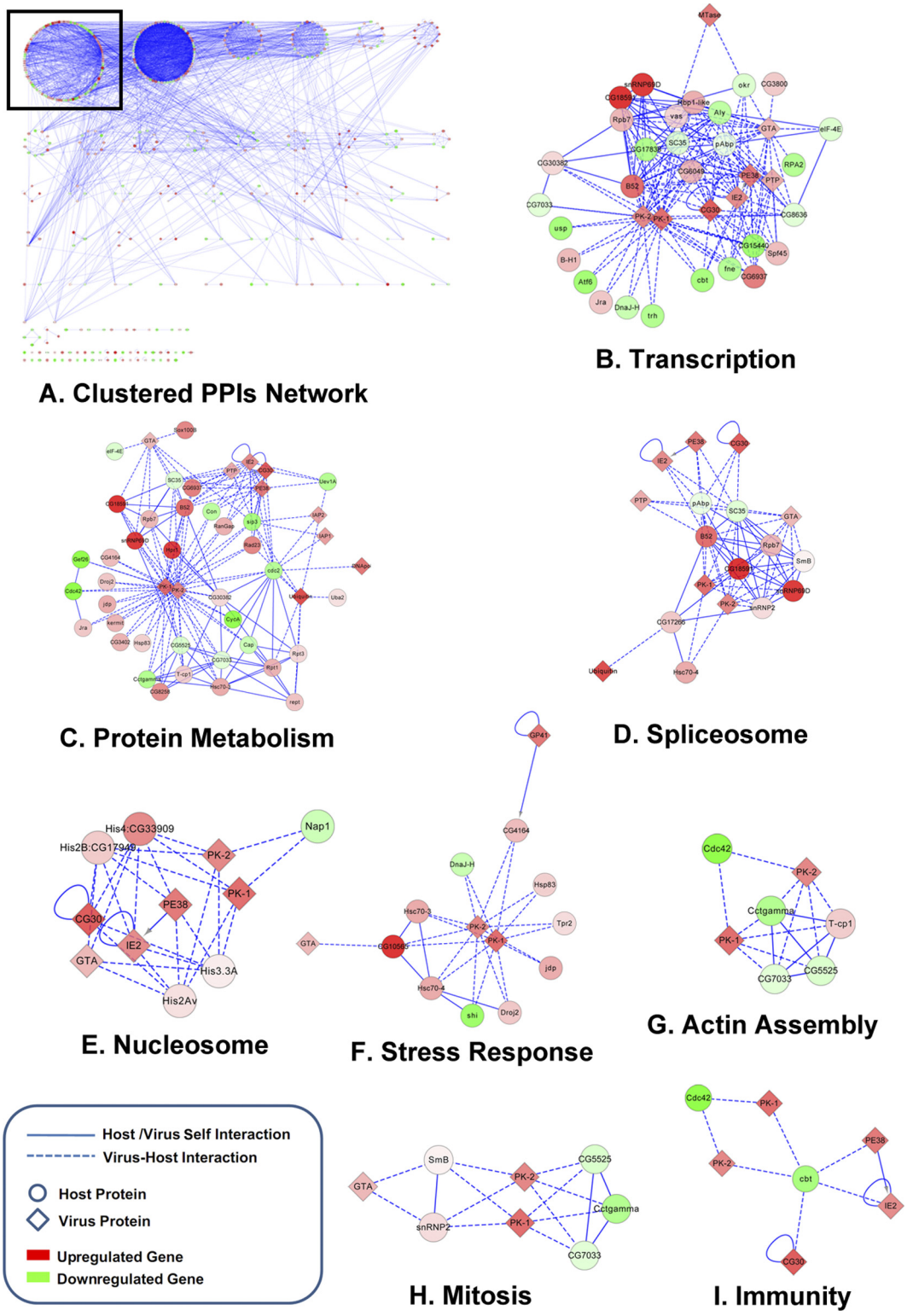

FIG 5 Subnetwork of virus-host PPIs in 24 hpi. The round nodes are host proteins, the diamond nodes are viral genes, and the color intensity of the nodes denotes the upregulation (red) or downregulation (green) of the genes at 24 hpi. The dashed lines indicate virus-host interactions. (A) Compact modular PPI network at 24 hpi. Virus-host PPI clusters were chosen for further analysis (black rectangle). (B through I) Subgroups for each functioned network module and its biological functions, suggesting that they formed protein complexes.

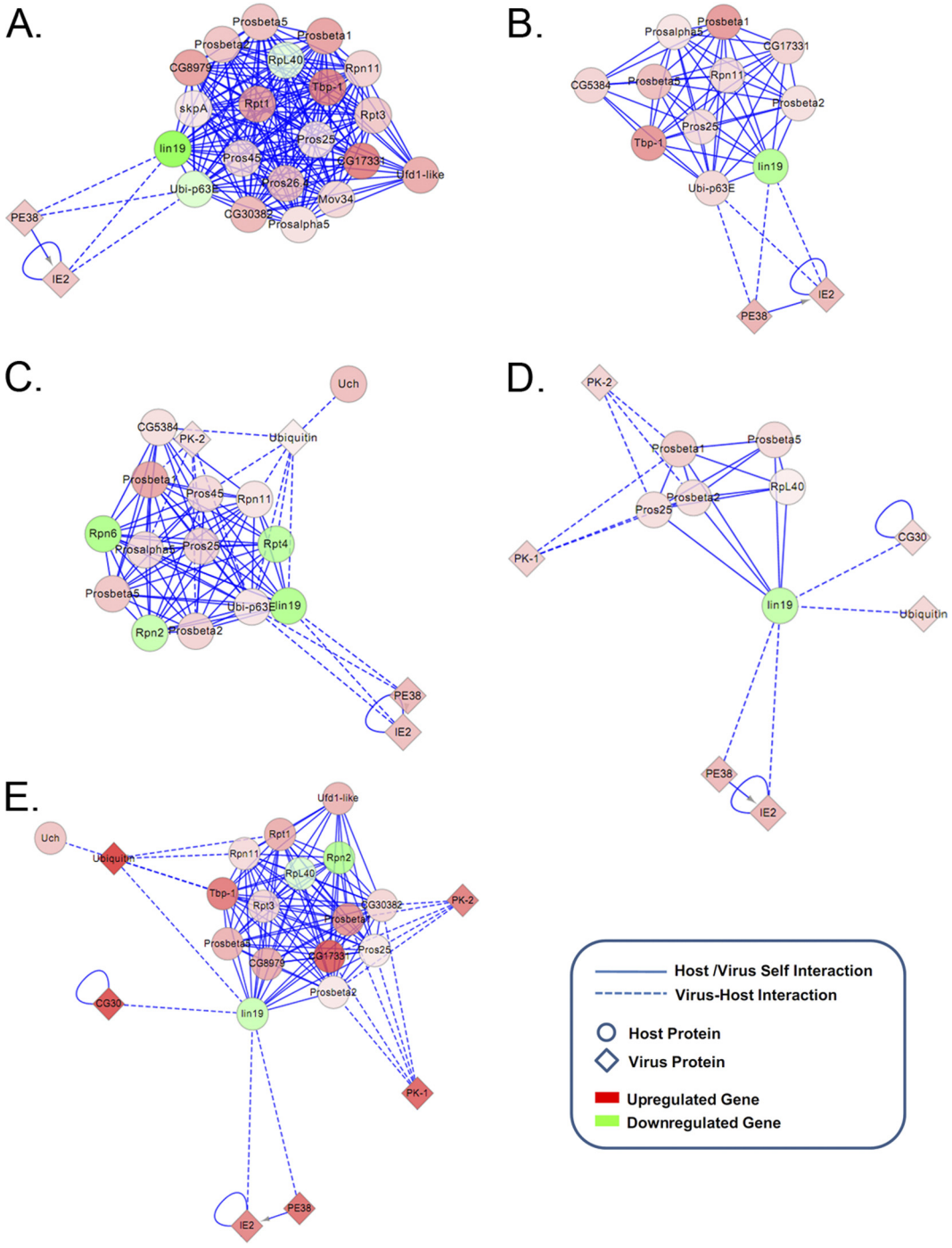

FIG 6 Viral proteins interact with the host ubiquitin-proteasome pathway. Based on virus-host PPI predictions and network function enriched with *P* value of <0.05, interactions between virus and the host ubiquitin-proteasome pathway-related genes were elucidated in a series of time courses, including 1.5 hpi (A), 3 hpi (B), 6 hpi (C), 12 hpi (D), and 24 hpi (E). The round nodes indicate host proteins, the diamond nodes are viral genes, and the color intensity of the nodes denotes the upregulation (red) or downregulation (green) of the indicated gene at 24 hpi. The dashed lines indicate the virus-host interactions.

dicted to interact with ubiquitin-proteasome pathway-related proteins (Fig. 6). Five of these viral proteins participated in transcription, indicating that the ubiquitin-proteasome pathway may play a key role in transcription during viral infection. Moreover, we demonstrated that BV and viral genome production was dramatically decreased in response to PS-341 treatment both *in vitro* and *in vivo*. And transcription of viral genes was strongly restricted after proteasome activity was inhibited. These results suggest that the ubiquitin-proteasome pathway plays a key role in BmNPV infection.

Iron ion metabolism participates in BmNPV replication. Iron ion metabolism is associated with the entry of the virus into

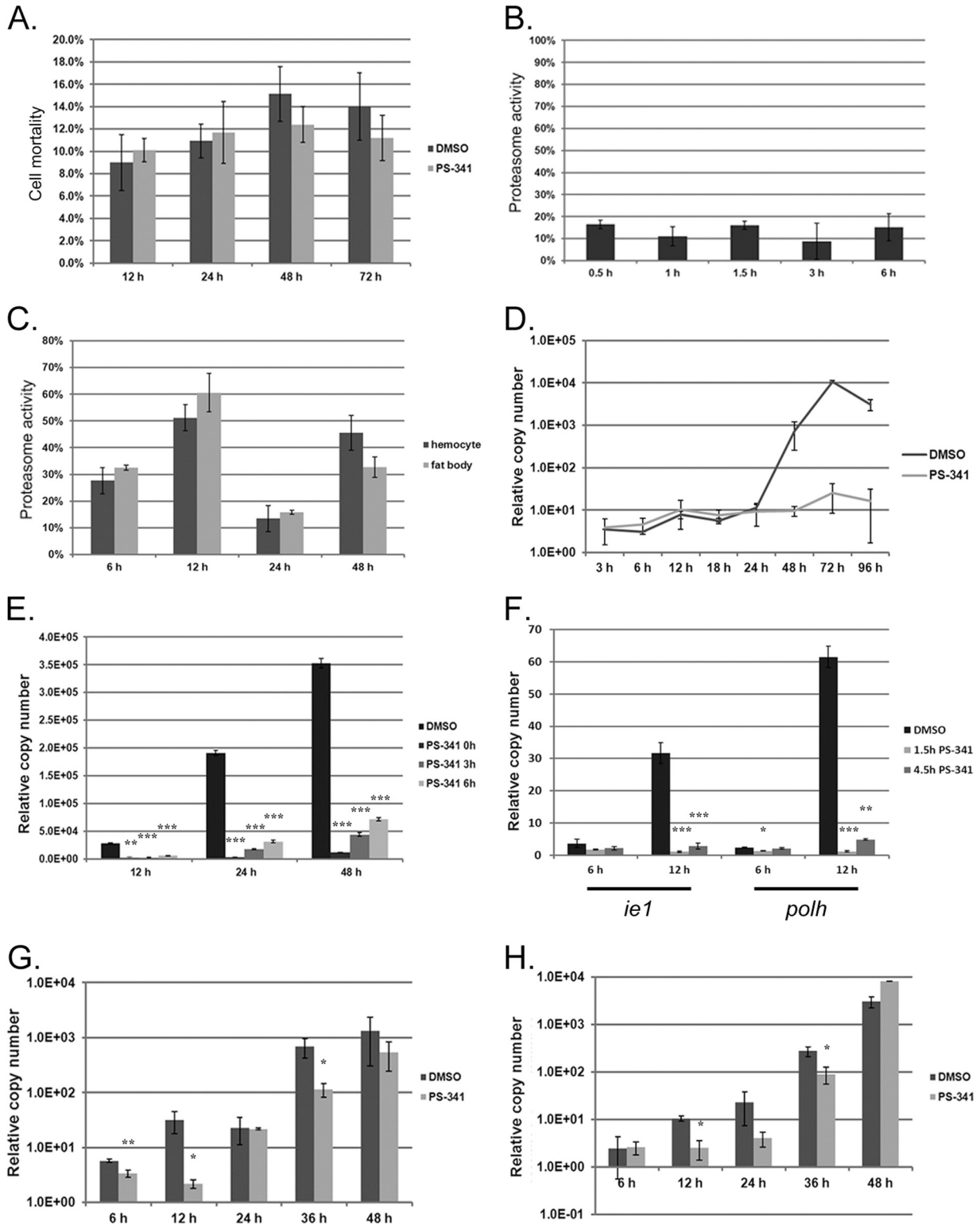

FIG 7 Proteasome activity assays and effects of proteasomal interactions during infection. (A) Bm5 cells were treated with PS-341 and DMSO, and cell mortality was calculated at 12, 24, 48, and 96 h posttreatment. Bm5 cells were stained with trypan blue for 2 min after treatment, and dead cells were counted in random visual fields. The percentage of nonviable cells is shown on the *y* axis. (B) Proteasome activity assay. Following treatment with PS-341 (5 μM) and DMSO over a time course, Bm5 cells were subjected to fluorometric measurement of 20S proteasome activity using Ys as a substrate (0.5 mM). Proteasome activity is shown as a percentage of the DMSO treatment at each time point on the *y* axis. (C) Proteasome activity assay of hemocytes and fat bodies. PS-341 and DMSO were injected into the fifth-instar silkworm larvae on the second day, and hemocytes and fat bodies were obtained and homogenized for proteasome activity assays. (D) BV relative copy numbers in the cell culture supernatants. Bm5 cells were infected with BmNPV T3 at an MOI of 10 and treated with DMSO or PS-341 (5 μM). Total DNA of BV was extracted at the indicated times after infection and subjected to qRT-PCR. (E) BmNPV proliferation in the Bm5 cells following treatment

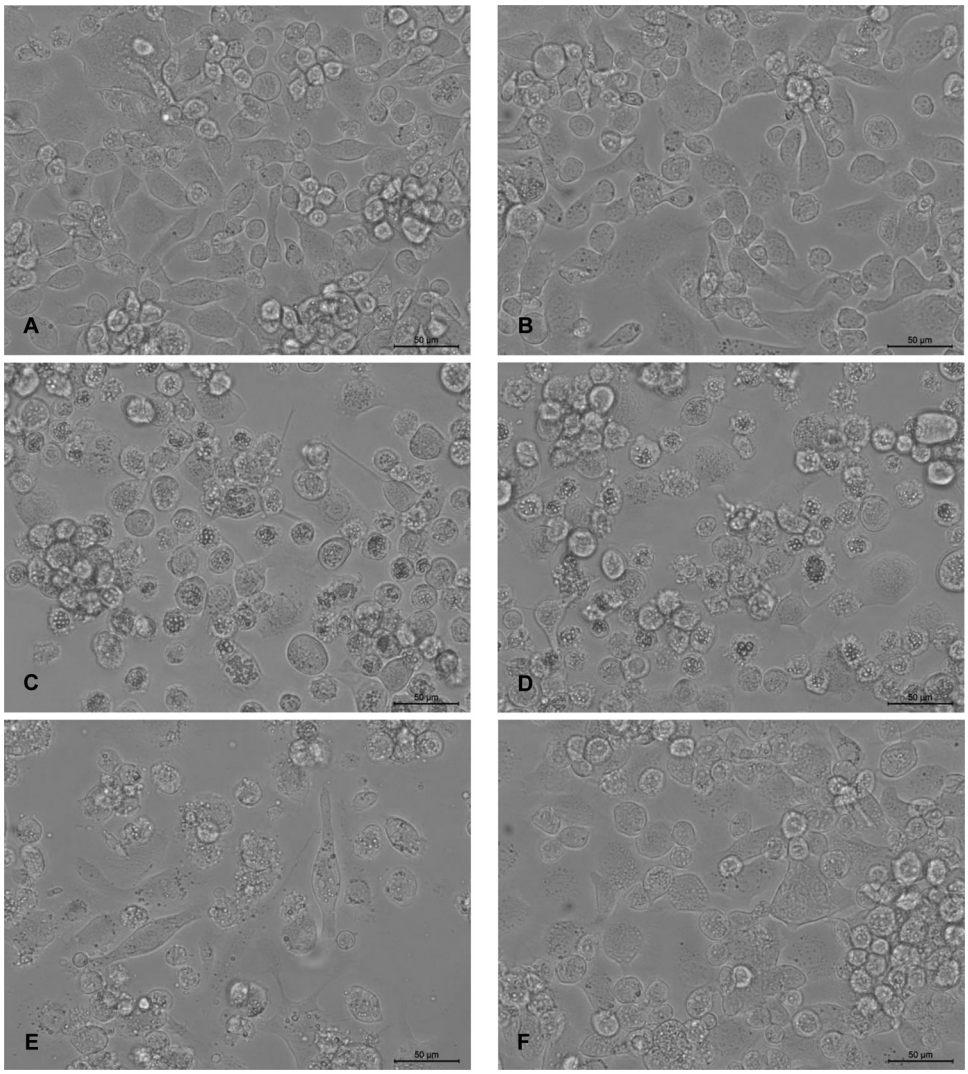

FIG 8 BmNPV infection conditions in Bm5 cells treated with PS-341 and DFO mesylate. Bm5 cells were treated for 48 h. (A) Uninfected cells (UIC) were treated with DMSO, as a negative control for PS-341 treatment. (B) UIC were treated with distilled water, as a negative control for DFO mesylate treatment. (C) Bm5 cells were infected with virus (MOI of 10) in the presence of DMSO. (D) Bm5 cells were infected with virus (MOI of 10) in the presence of distilled water. (E) Bm5 cells were infected with virus (MOI of 10) and treated with PS-341 (5 μM). (F) Bm5 cells were infected with virus (MOI of 10) and treated with DFO mesylate (5 mM). Scale bar, 50 μm.

the cell, virus replication, virus budding, and host antivirus strategy (14). In the present study, we observed that BmNPV replication was dramatically inhibited when iron ion was eliminated by DFO mesylate. However, by measuring viral genome copies at 1.5 hpi, we found that viral entry was not decreased with DFO treatment (data not shown), suggesting that iron ion is not associated with BmNPV entry. Moreover, we found that ferritin, which is responsible for the storage of ion in a soluble form in cells, was related to these gene sets. Furthermore, ferritin concentrations are known to increase in the presence of stress and infections (30, 42). Thus, it is reasonable to hypothesize that the BmNPV infection process requires the participation of iron ion and ferritin, which play key roles in iron ion metabolism in BmNPV-infected cells. However, this phenomenon requires further characterization.

Cell cycle regulation. Virus infection can cause cell cycle arrest during G_2/M (12). Previous studies indicate that baculovirus can

of PS-341 at 0, 3, and 6 hpi. Total DNA of Bm5 cells was extracted at 12, 24, and 48 hpi. Relative viral-DNA copy numbers were calculated, and *Bombyx GAPDH* gene expression served as an internal control. (F) Regulation of viral gene transcription following PS-341 treatment. After Bm5 cells were infected with BmNPV at an MOI of 10, PS-341 was added to cell culture supernatant at immediate-early and late viral gene expression start time points, 1.5 and 4.5 hpi, respectively. Total RNA was extracted from cells at 6 or 12 hpi. The RNA was then diluted 10-fold, and first-strand cDNA was subjected to qRT-PCR with specific primers for *ie1* and *polh*. (G) BmNPV proliferation in hemocytes with PS-341 treatment. PS-341 (10 μl of 0.5 mM PS-341 in DMSO per larva) was injected into the fifth-instar larvae for 1 day. Then, BmNPV viral suspension (10 μl) was injected into each larva after inhibitor treatment. Hemocytes were collected at 6, 12, 24, 36, and 48 hpi. Total DNA was extracted and subjected to qRT-PCR. (H) BmNPV proliferation in fat body with PS-341 treatment. Steps were followed as described above. Samples from each time point were tested independently and in triplicate. Pairwise statistical comparisons to the DMSO group were performed using Student's *t* test (*, $P \leq 0.05$; **, $P \leq 0.01$; ***, $P \leq 0.001$). Error bars indicate standard deviations ($n = 3$).

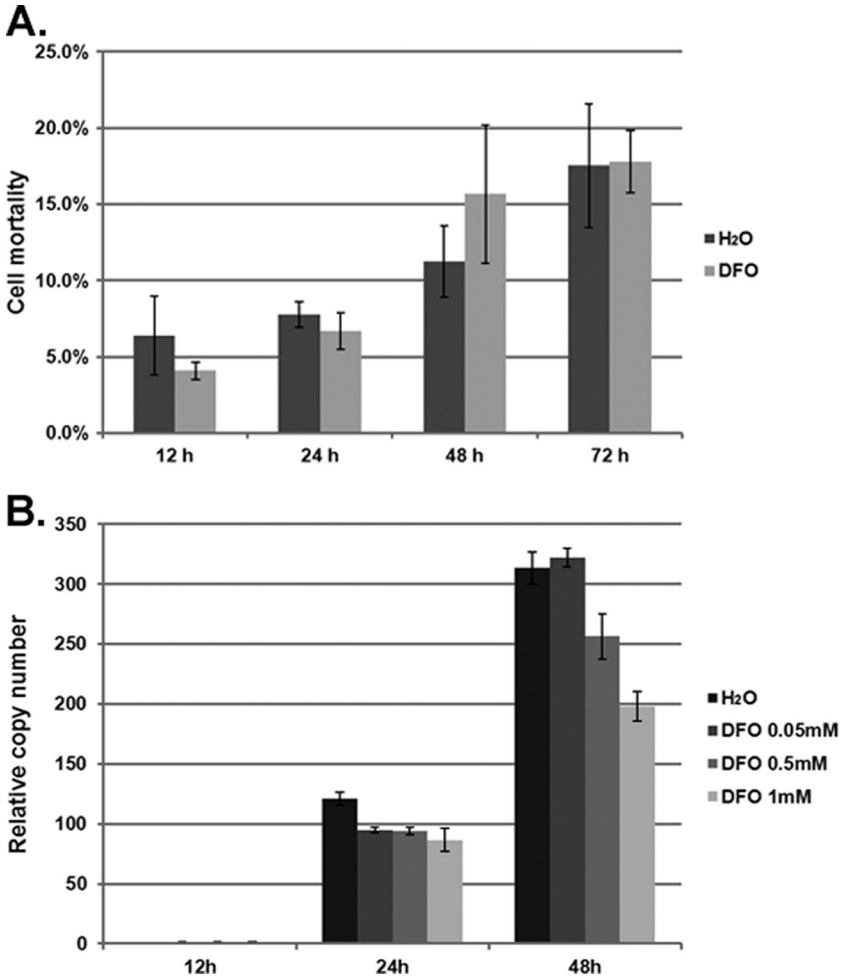

FIG 9 Viral-DNA replication in the presence of DFO mesylate.(A) Bm5 cells were treated with DFO (1 mM) and distilled water, and cell mortality was calculated at 12, 24, 48, and 96 h posttreatment. Bm5 cells were stained with trypan blue for 2 min after treatment, and dead cells were counted in random visual fields. The percentage of nonviable cells is shown on the *y* axis. (B) Dose-dependent inhibition of BmNPV T3 (MOI of 10) in Bm5 cells treated with distilled water or various concentrations of DFO mesylate (0.05, 0.5, and 1 mM). DNA was extracted at different time points postinfection (12, 24, 48, and 72 hpi). The relative viral-DNA copy numbers were calculated using *Bombyx GAPDH* gene expression as an internal control. Samples from each time point were tested independently and in triplicate. Error bars indicate standard deviations ($n = 3$).

arrest insect cell lines in the G_2/M and S phases, induced by viral genes *ie1* and *ie2*, and resulting in enlarged cells with high quantities of viral DNA (7, 51, 67). In our study, genes related to cell cycle and cell cycle arrest, namely, *cyclin B homolog*, *cullin-1*, and *14-3-3 epsilon*, were downregulated immediately after BmNPV infection. A cyclin B homolog, which was also predicted to interact with viral proteins, was immediately downregulated after BmNPV infection in our study. In contrast, Zhou et al. (67) have shown that a significant increase in cyclin B1 is able to induce cell cycle arrest at the G_2 phase. During G_2, cyclin B1 can accumulate and form a kinase complex with Cdk1. The active Cdk1/cyclin B1 complex plays a key role in the control of G_2/M cell cycle arrest (12). Cullin-1 is a component of Skp1/Cullin-1/F-box protein (SCF) complex. The SCF complex is required for degradation of Cdc25A, which prompted us to suspect that the modulation of Cullin-1 expression has an effect on the SCF-mediated degradation of Cdc25A during the S and G_2 phases (9, 13). Moreover, 14-3-3 epsilon binds to Cdc25 to keep the Cdk1/cyclin B1 complex inactive (12). At 6 and 12 hpi, the cell cycle pathway was significantly enriched in our network analysis, indicating that the host cell cycle can be modulated during the virus life cycle (see Table S7 in the supplemental material). The three previously mentioned upregulated genes are likely candidates for further study of cell cycle regulation.

Regulation of energy metabolism. The energy metabolism of insect cells is modulated after baculovirus infection (6, 10, 21, 43). Carinhas et al. (10) suggested that baculovirus production can be improved by manipulating energy metabolism. Iwanaga et al. (21) suggested that BmNPV-infected cells need more ATP for abrupt consumption. In our study, gene sets related to mitochondrial function were dramatically altered immediately after viral infection, which might affect mitochondrial respiration and apoptosis. These types of gene sets were highly upregulated in all of the postinfection time points (Table 2; see also Table S5 in the supplemental material). This finding is consistent with an earlier report indicating that energy metabolism-associated genes are overexpressed after BmNPV infection (21). Nevertheless, there is still a lack of knowledge about the role of cellular energy modulation

and baculovirus infection. In this study, we found that the regulation of energy metabolism genes might be a beneficial strategy for baculovirus infection.

RNA processing and remodeling. Baculovirus starts its infection cycle by employing enhancers and transcriptional activators of the host. These strategies focus on establishing viral infection and the production of key proteins necessary for its own replication and transcription (57). As shown in Fig. 3, host cell mRNA transcription gradually decreased by 24 hpi and showed a marked declined at 48 hpi. In contrast to previous reports (36, 60), the expression of most genes declined at 24 hpi, which was not shut down as quickly as in AcMNPV-infected Sf21 cells. Here, we observed a substantial number of differentially expressed genes at this time, considering that a second wave of viral infection and new virus assembly, which contribute to this phenomenon, might stimulate host gene regulation. In the present study, we found that gene sets related to translation initiation and cellular RNA synthesis were strongly modulated throughout the infection process, and some were predicted to interact with viral genes (Table 2 and Fig. 5B; see also Table S5 in the supplemental material). This finding might be due to the fact that the virus manipulates the translation and transcription resources of the host apparatus. To date, we cannot define the mechanism of host cell transcription inhibition. However, our study suggests that some host genes (data not shown), which are necessary and could facilitate viral gene transcription and translation, were upregulated, including a large number of ribosomal genes, *transcription initiation factor TFIID*, *3*, *1A*, *4A*, and *5A*, and elongation factor genes.

Heterogeneous nuclear ribonucleoproteins (hnRNPs) are complexes of RNA and proteins that shuttle between the nucleus and cytoplasm. hnRNPs bind to pre-mRNA molecules and serve as signals for the pre-mRNA metabolism process, transport, and localization. A total of seven viral proteins (CG30, GTA, IE2, PE38, PK-1, PK-2, and PTP) were predicted to interact with hnRNPs, namely, hnRNP A1, hnRNP H, and Squid (Sqd). hnRNP A1 and hnRNP H belong to the A/B hnRNPs subfamily, while Sqd is a type of hnRNP that is required for the regulation of grk and oskar mRNA nuclear export, localization, and translation during *Drosophila melanogaster* oogenesis (38, 39). In previous studies, these seven mediation viral proteins were mainly shown to be involved in gene transcription (11, 33), suggesting that viral pre-RNA might immediately bind to hnRNPs for metabolism and transport during transcription.

Some viruses (adenovirus, HIV, and herpesvirus) depend on cellular RNA splicing machinery for the expression of viral genes (16, 35, 37). Puvion-Dutilleul et al. (52) found that in response to adenoviral infection, the RNA processing machinery might play a role in the protection of virally spliced, polyadenylated mRNAs before exportation to the cytoplasm. Also, adenovirus infection can utilize cellular RNA splicing to produce a complex set of viral mRNAs during the infection process (2). Influenza virus nucleoprotein can bind to a cellular splicing factor, RAF-2p48, leading to enhanced viral RNA synthesis (34). In our study, spliceosome-related pathways were upregulated at 1.5 and 24 hpi (see Table S5 in the supplemental material), suggesting that the processing of BmNPV mRNA may depend on host RNA processing machinery. Protein interaction analysis also revealed that viral genes belong to transcription factors that can interact with spliceosome complex proteins, suggesting that the cellular spliceosome machinery may facilitate viral gene transcription and splicing (Fig. 5D). However, further investigation is necessary to determine how this pathway participates in the production of viral mRNA and limits host gene expression.

Chromatin regulation. Histones are a type of protein that packages and orders genomic DNA into nucleosomes and is a main component of chromatin. Interestingly, our results indicated that gene sets related to the nucleosome were upregulated, including five histone genes (BmV09147, BmV03398, BmV00407, BmV03559, and BmV04674). The increased expression of histone proteins may be involved in regulating the host chromatin structure, which could create a barrier to some biological pathways, such as DNA replication, transcription, and recombination. The recruitment and dynamic modification of histone proteins are also promoted by cytomegalovirus to regulate viral gene expression (53). Placek and Berger (50) reported that host histone can also package the genome of herpes simplex virus 1 (HSV-1). However, the relationships between host histone overexpression and baculovirus infection are unclear. Moreover, network analysis revealed enrichment in virus-host protein interactions (at 3, 6, 12, and 24 hpi) between gene sets related to the nucleosome and chromosome assembly (Fig. 5E; see also Table S7 in the supplemental material). Surprisingly, all of the histone genes that we found to be modulated were predicted to interact with viral proteins. One possible explanation is that host transcription is inhibited by chromatin regulation, and histones could also be utilized to promote viral gene expression.

Interactions between viral proteins and cytoskeleton-related proteins. The actin cytoskeleton of host cells is known to facilitate baculovirus motility, translocation, transcription, and BV and occlusion-derived virus (ODV) formation (32, 40, 63). In our study, two viral proteins (PK-1 and PK-2) are predicted to interact with actin filament polymerization and chaperonin-containing T-complex-related proteins (Cdc42, Cctgamma, T-cp1, CG7033, and CG5525), which are required for cytoplasmic microtubule organization. PK-1 and PK-2 proteins are homologous to eukaryotic protein kinases, which might associate to the enzymatic activity of these host proteins (54). A previous study also showed that the viral Arif-1 is tyrosine phosphorylated and involved in the remodeling of the actin cytoskeleton, but it has not been shown that PK-1 phosphorylates Arif-1 (15). These data suggest that viral infection could change the enzymatic activity of these actin organizers to affect actin filament polymerization and act as mediators to influence gene transcription (Fig. 5G). These results indicate an unsuspected role for the cytoskeleton in the regulation of baculovirus gene transcription.

The immune pathway in relation to the viral process. The MAPK signaling pathway and JNK cascade were identified as participating in BmNPV infection (27). Our interaction network also suggested that the immune pathway affects five viral transcriptional proteins that could interact with Ras85D, including Pointed (*pnt*), Cabut (*cbt*), and cell division cycle 42 (Cdc42, a Rho-GTPase). Considering the role of MAPK and JNK signaling pathways for efficient BmNPV infection, these data suggest that the virus can utilize the immune pathway for facilitating expression of its own genes (27).

Viral genes mediate interactions between the virus and host. To date, few baculovirus proteins have been reported to interact with host proteins (8, 18, 45). Considering that most known interactions are dedicated to the characterization of viral proteins, few host protein-associations have been reported. In the present study, for BmNPV, a total of 22 viral proteins were predicted to interact with host proteins.

From network module analysis of the virus-host PPI network, we found that viral genes dynamically mediate different functions of host genes. For example, autophosphorylation and the ubiquitin-proteasome pathway are enriched at the initial stages of infection (1.5 hpi) (see Table S7 in the supplemental material). During this time, viruses enter into cells and face competition with well-organized cellular machineries. At 6 hpi, as viral genes increase expression, genes related to the ubiquitin-proteasome pathway, protein modification process, chromatin, and cell cycle are enriched (see Table S7 in the supplemental material). Meanwhile, we found that myosin genes also participated in viral gene interactions. Pestic-Dragovich et al. (48) suggested that a nuclear isoform of myosin I β (nuclear myosin 1) exists in a complex with RNA polymerase II and affects gene transcription. Similar to actin, both of them are associated with ribosomal DNA (rDNA) transcription and are necessary for RNA polymerase I transcription (49). Thus, baculovirus might take advantage of interactions with myosin genes to control host gene expression. As the infection proceeds from 12 to 24 hpi, most of the protein interaction is related to the functions of mRNA metabolic processes, the ribonucleoproteins (RNP) complex, cell response to stress, nucleosome assembly, and actin filament polymerization (see Table S7 in the supplemental material). Functional analysis of this module showed that viral genes participate in the host RNA splicing machinery. Our results also confirmed that actin is associated with gene transcription, especially RNP particles, and it is associated with the regulation of chromatin structure (46). Protein interactions of this module explain the high expression of viral genes during this interval. At the end of the viral infection cycle (48 and 96 hpi), most of the host genes are downregulated, and no module emerged between viral and host proteins. This result indicates that virion assembly in the late infection stage has less help from host proteins.

According to our results, five viral proteins showed approximately 1,000 interactions with host proteins. All of these viral proteins are involved in transcriptional functions (PK-1, PK-2, CG30, IE2, and PE38), suggesting that their interactions might play a key role in viral gene transcription. Additionally, some other viral proteins that interacted with host proteins remain undefined. For example, the viral proteins IAPs were reported to block virus-induced apoptosis (61). In this study, we found that IAPs interact with the serine/threonine-protein kinase, polo, which is required for mitosis in *Drosophila* (31). Thus, IAPs could affect host mitosis through PPIs. A viral protein, SOD, is a homolog of a host protein that is essential for viral replication and might mitigate the effects of superoxide production by hemocytes. Furthermore, we predicted that SOD could interact with the host protein myosin light polypeptide 9 isoform B, which may be involved in other processes during infection. Methyltransferase (MTase) was observed to participate in gene transcription and translation according to our predicted PPI network.

Additionally, we identified 335 BV-associated cellular proteins, using LTQ Orbitrap (data not shown). A total of 92 proteins were predicted to interact with 18 viral genes. Meanwhile, some host proteins were also detected in AcMNPV BV, such as actin, 14-3-3 zeta protein, Rab11, and annexin (64). Additionally, some host proteins were included in the mass spectrometry results, such as histone proteins (Hist1h4c and histone H2A-like protein 2), cell cycle proteins (14-3-3 epsilon protein and cullin-1), and cytoskeletal proteins (actin).

This virus-host PPI network could provide clues to aid in the understanding of the viral infection process and the interactions between the virus and host at a systematic level. We identified a larger number of interactions between cellular components and virus than was anticipated, and the proteins that we analyzed are important for the transfer of information between the virus and its target proteins. The predicted virus-host protein interactions identified in this study extend our knowledge of the viral infection process and indicate novel functions for several viral genes.

In summary, we comprehensively analyzed changes in the gene expression pattern of host cells after viral infection by using next-generation sequencing. Additionally, we are the first to define an interactome between BmNPV and host proteins at a systematic level. Our data strongly suggest that BmNPV can fully utilize the host cellular machinery for successful infection. This work provides a global view of the host response during infection that not only is consistent with previous studies but also provides new insights into the interaction between virus and host during infection. Overall, this work increases our understanding of the baculovirus infection process.

ACKNOWLEDGMENTS

This work was supported by grants from the National Natural Science Foundation of China (31070136 and 30570074) and the National Basic Research Program of China (973 Program, No. 2010CB126200).

REFERENCES

1. **Adams J, et al.** 1999. Proteasome inhibitors: a novel class of potent and effective antitumor agents. Cancer Res. **59**:2615–2622.
2. **Akusjarvi G, Stevenin J.** 2003. Remodelling of the host cell RNA splicing machinery during an adenovirus infection. Curr. Top. Microbiol. Immunol. **272**:253–286.
3. **Ansorge WJ.** 2009. Next-generation DNA sequencing techniques. Nat. Biotechnol. **25**:195–203.
4. **Bao YY, et al.** 2010. Comparative analysis of Bombyx mori nucleopolyhedrovirus responsive genes in fat body and haemocyte of B. mori resistant and susceptible strains. Insect Mol. Biol. **19**:347–358.
5. **Bao YY, et al.** 2009. Gene expression profiling of resistant and susceptible Bombyx mori strains reveals nucleopolyhedrovirus-associated variations in host gene transcript levels. Genomics **94**:138–145.
6. **Bernal V, Carinhas N, Yokomizo AY, Carrondo MJ, Alves PM.** 2009. Cell density effect in the baculovirus-insect cells system: a quantitative analysis of energetic metabolism. Biotechnol. Bioeng. **104**:162–180.
7. **Braunagel SC, Parr R, Belyavskyi M, Summers MD.** 1998. Autographa californica nucleopolyhedrovirus infection results in Sf9 cell cycle arrest at G2/M phase. Virology **244**:195–211.
8. **Braunagel SC, Summers MD.** 2007. Molecular biology of the baculovirus occlusion-derived virus envelope. Curr. Drug Targets **8**:1084–1095.
9. **Busino L, et al.** 2003. Degradation of Cdc25A by beta-TrCP during S phase and in response to DNA damage. Nature **426**:87–91.
10. **Carinhas N, et al.** 2010. Improving baculovirus production at high cell density through manipulation of energy metabolism. Metab. Eng. **12**:39–52.
11. **Carstens EB, Liu JJ, Dominy C.** 2002. Identification and molecular characterization of the baculovirus CfMNPV early genes: ie-1, ie-2 and pe38. Virus Res. **83**:13–30.
12. **Davy C, Doorbar J.** 2007. G2/M cell cycle arrest in the life cycle of viruses. Virology **368**:219–226.
13. **Donzelli M, et al.** 2002. Dual mode of degradation of Cdc25 A phosphatase. EMBO J. **21**:4875–4884.
14. **Drakesmith H, Prentice A.** 2008. Viral infection and iron metabolism. Nat. Rev. Microbiol. **6**:541–552.
15. **Dreschers S, Roncarati R, Knebel-Morsdorf D.** 2001. Actin rearrangement-inducing factor of baculoviruses is tyrosine phosphorylated and colocalizes to F-actin at the plasma membrane. J. Virol. **75**:3771–3778.
16. **Fukuhara T, et al.** 2006. Utilization of host SR protein kinases and RNA-splicing machinery during viral replication. Proc. Natl. Acad. Sci. U. S. A. **103**:11329–11333.
17. **Gao G, Luo H.** 2006. The ubiquitin-proteasome pathway in viral infections. Can. J. Physiol. Pharmacol. **84**:5–14.

18. **Goley ED, et al.** 2006. Dynamic nuclear actin assembly by Arp2/3 complex and a baculovirus WASP-like protein. Science **314**:464–467.
19. **Gomi S, Majima K, Maeda S.** 1999. Sequence analysis of the genome of Bombyx mori nucleopolyhedrovirus. J. Gen. Virol. **80**(Pt 5):1323–1337.
20. **Hayakawa T, Rohrmann GF, Hashimoto Y.** 2000. Patterns of genome organization and content in lepidopteran baculoviruses. Virology **278**:1–12.
21. **Iwanaga M, Shimada T, Kobayashi M, Kang WK.** 2007. Identification of differentially expressed host genes in Bombyx mori nucleopolyhedrovirus infected cells by using subtractive hybridization. Appl. Entomol. Zool. **42**:151–159.
22. **Jensen LJ, et al.** 2009. STRING 8—a global view on proteins and their functional interactions in 630 organisms. Nucleic Acids Res. **37**:D412–D416.
23. **Jung T, Catalgol B, Grune T.** 2009. The proteasomal system. Mol. Aspects Med. **30**:191–296.
24. **Kanehisa M, Goto S.** 2000. KEGG: Kyoto encyclopedia of genes and genomes. Nucleic Acids Res. **28**:27–30.
25. **Kanlaya R, Pattanakitsakul SN, Sinchaikul S, Chen ST, Thongboonkerd V.** 2010. The ubiquitin-proteasome pathway is important for dengue virus infection in primary human endothelial cells. J. Proteome Res. **9**:4960–4971.
26. **Katsuma S, Kawaoka S, Mita K, Shimada T.** 2008. Genome-wide survey for baculoviral host homologs using the Bombyx genome sequence. Insect Biochem. Mol. Biol. **38**:1080–1086.
27. **Katsuma S, Mita K, Shimada T.** 2007. ERK- and JNK-dependent signaling pathways contribute to Bombyx mori nucleopolyhedrovirus infection. J. Virol. **81**:13700–13709.
28. **Katsuma S, Shimada T, Kobayashi M.** 2004. Characterization of the baculovirus Bombyx mori nucleopolyhedrovirus gene homologous to the mammalian FGF gene family. Virus Genes **29**:211–217.
29. **Kost TA, Condreay JP, Jarvis DL.** 2005. Baculovirus as versatile vectors for protein expression in insect and mammalian cells. Nat. Biotechnol. **23**:567–575.
30. **Larade K, Storey KB.** 2004. Accumulation and translation of ferritin heavy chain transcripts following anoxia exposure in a marine invertebrate. J. Exp. Biol. **207**:1353–1360.
31. **Llamazares S, et al.** 1991. polo encodes a protein kinase homolog required for mitosis in Drosophila. Genes Dev. **5**:2153–2165.
32. **Marek M, Merten OW, Galibert L, Vlak JM, van Oers MM.** 2011. Baculovirus VP80 protein and the F-actin cytoskeleton interact and connect the viral replication factory with the nuclear periphery. J. Virol. **85**:5350–5362.
33. **Mishra G, Chadha P, Das RH.** 2008. Serine/threonine kinase (pk-1) is a component of Autographa californica multiple nucleopolyhedrovirus (AcMNPV) very late gene transcription complex and it phosphorylates a 102 kDa polypeptide of the complex. Virus Res. **137**:147–149.
34. **Momose F, et al.** 2001. Cellular splicing factor RAF-2p48/NPI-5/BAT1/UAP56 interacts with the influenza virus nucleoprotein and enhances viral RNA synthesis. J. Virol. **75**:1899–1908.
35. **Muhlemann O, Yue BG, Petersen-Mahrt S, Akusjarvi G.** 2000. A novel type of splicing enhancer regulating adenovirus pre-mRNA splicing. Mol. Cell. Biol. **20**:2317–2325.
36. **Nobiron I, O'Reilly DR, Olszewski JA.** 2003. Autographa californica nucleopolyhedrovirus infection of Spodoptera frugiperda cells: a global analysis of host gene regulation during infection, using a differential display approach. J. Gen. Virol. **84**:3029–3039.
37. **Nojima T, et al.** 2009. Herpesvirus protein ICP27 switches PML isoform by altering mRNA splicing. Nucleic Acids Res. **37**:6515–6527.
38. **Norvell A, Debec A, Finch D, Gibson L, Thoma B.** 2005. Squid is required for efficient posterior localization of oskar mRNA during Drosophila oogenesis. Dev. Genes Evol. **215**:340–349.
39. **Norvell A, Kelley RL, Wehr K, Schupbach T.** 1999. Specific isoforms of squid, a Drosophila hnRNP, perform distinct roles in Gurken localization during oogenesis. Genes Dev. **13**:864–876.
40. **Ohkawa T, Volkman LE, Welch MD.** 2010. Actin-based motility drives baculovirus transit to the nucleus and cell surface. J. Cell Biol. **190**:187–195.
41. **Okano K, Shimada T, Mita K, Maeda S.** 2001. Comparative expressed-sequence-tag analysis of differential gene expression profiles in BmNPV-infected BmN cells. Virology **282**:348–356.
42. **Ong DS, Wang L, Zhu Y, Ho B, Ding JL.** 2005. The response of ferritin to LPS and acute phase of Pseudomonas infection. J. Endotoxin Res. **11**:267–280.
43. **Palomares LA, Lopez S, Ramirez OT.** 2004. Utilization of oxygen uptake rate to assess the role of glucose and glutamine in the metabolism of infected insect cell cultures. Biochem. Eng. J. **19**:87–93.
44. **Pederson T, Aebi U.** 2005. Nuclear actin extends, with no contraction in sight. Mol. Biol. Cell **16**:5055–5060.
45. **Peng K, et al.** 2010. Identification of protein-protein interactions of the occlusion-derived virus-associated proteins of Helicoverpa armigera nucleopolyhedrovirus. J. Gen. Virol. **91**:659–670.
46. **Percipalle P, Visa N.** 2006. Molecular functions of nuclear actin in transcription. J. Cell Biol. **172**:967–971.
47. **Pertea G, et al.** 2003. TIGR Gene Indices Clustering Tools (TGICL): a software system for fast clustering of large EST datasets. Bioinformatics **19**:651–652.
48. **Pestic-Dragovich L, et al.** 2000. A myosin I isoform in the nucleus. Science **290**:337–341.
49. **Philimonenko VV, et al.** 2004. Nuclear actin and myosin I are required for RNA polymerase I transcription. Nat. Cell Biol. **6**:1165–1172.
50. **Placek BJ, Berger SL.** 2010. Chromatin dynamics during herpes simplex virus-1 lytic infection. Biochim. Biophys. Acta **1799**:223–227.
51. **Prikhod'ko EA, Miller LK.** 1998. Role of baculovirus IE2 and its RING finger in cell cycle arrest. J. Virol. **72**:684–692.
52. **Puvion-Dutilleul F, Bachellerie JP, Visa N, Puvion E.** 1994. Rearrangements of intranuclear structures involved in RNA processing in response to adenovirus infection. J. Cell Sci. **107**(Pt 6):1457–1468.
53. **Reeves MB.** 2011. Chromatin-mediated regulation of cytomegalovirus gene expression. Virus Res. **157**:134–143.
54. **Reilly LM, Guarino LA.** 1994. The pk-1 gene of Autographa californica multinucleocapsid nuclear polyhedrosis virus encodes a protein kinase. J. Gen. Virol. **75**(Pt 11):2999–3006.
55. **Robinson MD, McCarthy DJ, Smyth GK.** 2010. edgeR: a Bioconductor package for differential expression analysis of digital gene expression data. Bioinformatics **26**:139–140.
56. **Rohrmann GF.** 26 January 2011, posting date. Chapter 1. Introduction to the baculoviruses, their taxonomy, and evolution. *In* Rohrmann GF (ed), Baculovirus molecular biology, 2nd ed. National Center for Biotechnology Information, Bethesda, MD.
57. **Rohrmann GF.** 26 January 2011, posting date. Chapter 3. The baculovirus replication cycle: effects on cells and insects. *In* Rohrmann GF (ed), Baculovirus molecular biology, 2nd ed. National Center for Biotechnology Information, Bethesda, MD.
58. **Rohrmann GF.** 26 January 2011, posting date. Chapter 8. Host resistance and susceptibility. *In* Rohrmann GF (ed), Baculovirus molecular biology, 2nd ed. National Center for Biotechnology Information, Bethesda, MD.
59. **Sagisaka A, et al.** 2010. Genome-wide analysis of host gene expression in the silkworm cells infected with Bombyx mori nucleopolyhedrovirus. Virus Res. **147**:166–175.
60. **Salem TZ, Zhang F, Xie Y, Thiem SM.** 2011. Comprehensive analysis of host gene expression in Autographa californica nucleopolyhedrovirus-infected Spodoptera frugiperda cells. Virology **412**:167–178.
61. **Seshagiri S, Miller LK.** 1997. Baculovirus inhibitors of apoptosis (IAPs) block activation of Sf-caspase-1. Proc. Natl. Acad. Sci. U. S. A. **94**:13606–13611.
62. **Tweedie S, et al.** 2009. FlyBase: enhancing Drosophila Gene Ontology annotations. Nucleic Acids Res. **37**:D555–D559.
63. **Volkman LE.** 2007. Baculovirus infectivity and the actin cytoskeleton. Curr. Drug Targets **8**:1075–1083.
64. **Wang R, et al.** 2010. Proteomics of the Autographa californica nucleopolyhedrovirus budded virions. J. Virol. **84**:7233–7242.
65. **Xia K, Dong D, Han JD.** 2006. IntNetDB v1.0: an integrated protein-protein interaction network database generated by a probabilistic model. BMC Bioinformatics. **7**:508. doi:10.1186/1471-2105-7-508.
66. **Xia K, Fu Z, Hou L, Han JD.** 2008. Impacts of protein-protein interaction domains on organism and network complexity. Genome Res. **18**:1500–1508.
67. **Zhou R, et al.** 2004. Heliocoverpa armigera single nucleocapsid nucleopolyhedrovirus induces Hz-AM1 cell cycle arrest at the G2 phase with accumulation of cyclin B1. Virus Res. **105**:113–120.
68. **Zou W, et al.** 2006. Vitamin C inactivates the proteasome inhibitor PS-341 in human cancer cells. Clin. Cancer Res. **12**:273–280.